

# Assessment of Improved Nonlinear Static Procedures in FEMA-440

Sinan Akkar<sup>1</sup> and Asli Metin<sup>2</sup>

**Abstract:** Nonlinear static procedures (NSPs) presented in the FEMA-440 document are evaluated for nondegrading three- to nine-story reinforced concrete moment-resisting frame systems. Evaluations are based on peak single-degree-of-freedom displacement, peak roof, and interstory drifts estimations. A total of 78 soil site records and 24 buildings with fundamental periods varying between 0.3 s–1.3 s are used in 2,832 linear and nonlinear response-history analyses to derive the descriptive statistics. The moment magnitude of the ground motions varies between 5.7 and 7.6. All records are within 23 km of the causative fault representing near-fault ground motions with and without pulse signals. The statistics presented suggest that lateral loading patterns used in pushover analysis to idealize the building systems play a role in the accuracy of NSPs investigated. Both procedures yield fairly good deformation demand estimations on the median. Displacement coefficient method (DCM) tends to overestimate the global deformation demands with respect to the capacity spectrum method (CSM). The conservative deformation demand estimations of DCM are correlated with the normalized lateral strength ratio,  $R$ . The CSM tends to overestimate the deformation demands for the increasing displacement ductility,  $\mu$ .

**DOI:** 10.1061/(ASCE)0733-9445(2007)133:9(1237)

**CE Database subject headings:** Seismic effects; Drift; Approximation methods; Performance characteristics; Frames; Statistics.

## Introduction

The response of structural systems under strong ground shaking generally results in nonlinear behavior. Until recently, retrofitting techniques relied on linear analysis to predict the structural response against earthquakes. However, the increased implementation of displacement-based seismic assessment of structures led to the proposition of approximate nonlinear static procedures (NSPs) for the prediction of seismic structural behavior. The nonlinear methods published in the ATC-40 (ATC 1996) report together with the FEMA-273/274 (BSSC 1997) documents and the successor FEMA-356 (ASCE 2000) report constitute the well-organized pioneer representatives in this field. The basic premise in these procedures is the estimation of deformation demands on structural systems by making use of nonlinear force-deformation curves that are generated from pushover analysis. This initial step reduces the multidegree-of-freedom (MDOF) system to an idealized single-degree-of-freedom (SDOF) system, thus, simplifying the structural model, as well as providing insightful information about the likely nonlinear behavior of the structure. While this initial step is common for the above documents, the ATC-40 document primarily details the capacity spectrum method (CSM). This method is

an equivalent linear technique that uses displacement ductility ( $\mu$ ) based empirical relationships to approximate the nonlinear response of the SDOF system through an equivalent linear oscillator by elongating the period and increasing the viscous damping. The FEMA-356 report describes the displacement coefficient method (DCM) in which several empirically derived factors are used to modify the elastic response of the SDOF system for estimating the nonlinear behavior. The empirical factors used in the DCM are primarily based on the lateral yield strength of the system.

These two procedures have been recently updated by the project ATC-55 that is principally aimed to improve the accuracy of the peak SDOF displacement estimations. The regression equations used in the improved DCM for estimating the expected peak inelastic SDOF displacements were derived from the statistical study conducted by Ruiz-García and Miranda (2003). The ductility dependent empirical relations used in the improved CSM were presented by Guyader and Iwan (2006). The principal product of the ATC-55 project is the FEMA-440 (ATC 2005) report that presents the improved versions of the DCM and CSM, as well as a limited comparative study providing a preliminary evaluation of these methods. The comparative results were confined to nine distinct bilinear oscillators with periods of 0.2 s, 0.5 s, and 1.0 s that were subjected to 13 strong ground motions. The analyses indicated that the mean SDOF deformation demand estimations of the improved NSPs follow a fairly close pattern to the mean deformation demands computed from the nonlinear response-history analyses (RHA).

A recent study by Kazaz et al. (2006) investigated the accuracy of the improved CSM for a significantly stiff, high-lateral strength, wall-type structure subjected to 55 near- and far-fault ground motions recorded on rock sites. The mean error statistics depicted by Kazaz et al. (2006) reported an average of 20% unsafe peak SDOF displacement predictions with respect to the nonlinear RHA results. Using a comprehensive ground-motion

<sup>1</sup>Associate Professor, Earthquake Engineering Research Center, Middle East Technical Univ., 06531 Ankara, Turkey. E-mail: sakkar@metu.edu.tr

<sup>2</sup>Structural Engineer, Coyne and Bellier Engineering and Consultancy, 06520 Ankara, Turkey.

Note. Associate Editor: Rakesh K. Goel. Discussion open until February 1, 2008. Separate discussions must be submitted for individual papers. To extend the closing date by one month, a written request must be filed with the ASCE Managing Editor. The manuscript for this paper was submitted for review and possible publication on April 12, 2006; approved on February 27, 2007. This paper is part of the *Journal of Structural Engineering*, Vol. 133, No. 9, September 1, 2007. ©ASCE, ISSN 0733-9445/2007/9-1237-1246/\$25.00.

database and wide-range spectral periods, Akkar and Miranda (2005) also conducted a statistical study on the accuracy of the methods proposed by Guyader and Iwan (2006) and Ruiz-García and Miranda (2003). Akkar and Miranda (2005) indicated that for elastoplastic behavior, on average, both methods would yield substantially different estimations when vibration periods are less than approximately 0.6 s. The discrepancy between these methods becomes more apparent for decreasing lateral strength capacities having a tendency toward a significant overestimation for the equivalent linear method proposed by Guyader and Iwan (2006). This observation is contradictory to the conclusions made by Kazaz et al. (2006), as they reported unsafe predictions by the improved CSM. The reason behind such conflicting results might emerge from different scenarios put forward during the evaluation of the NSPs. While Kazaz et al. (2006) established their results using an idealized SDOF system of a high-strength capacity, very stiff, wall-type structure, Akkar and Miranda (2005) used generic elastoplastic oscillators to compute the relevant statistics as a function of a normalized lateral strength and vibration period.

This study evaluates the improved NSPs presented in FEMA-440 by using a common building inventory and ground-motion database with a total of 24 nondegrading, three- to nine-story reinforced concrete (RC) moment-resisting frames and 78 stiff soil near-fault records. The accuracy of the NSPs was verified for peak SDOF displacement, maximum roof, and interstory drifts. The frame models conform to modern seismic design codes that ensure nondeteriorating cyclic behavior in strength. The nondeteriorating lateral strength hysteretic behavior leads the study to evaluate the common points in the improved NSPs, as both procedures describe strength deterioration by different hysteretic models that would result in biased comparisons within the context of this study. The statistics presented suggest that the accuracy of NSPs is sensitive to the changes in the lateral strength capacity, ductility demand, and postyield stiffness. Different lateral loading patterns also influence the degree of accuracy of the NSPs investigated.

## Ground-Motion Database

The moment magnitude ( $M$ ) ( $5.7 < M < 7.6$ ) and the shortest source-to-site distance ( $1 \text{ km} < d < 23 \text{ km}$ ) distribution of the ground-motion database exhibit the features of the moderate-to-severe near-fault events. Almost all of the ground motions (75 records out of 78) are recordings from stiff soil sites with an average shear-wave velocity of  $360 \text{ m/s} < V_s < 760 \text{ m/s}$  in the upper 30 m. The ground-motion database was subdivided into four bins to emphasize the amplitude variation in the ground velocity and the pulse-type waveform feature that are used to parameterize the near-fault influence on structures (Bray and Rodriguez-Marek 2004). Groups A and B consist of 20 near-fault records with  $40 \text{ cm/s} < \text{peak ground velocity (PGV)} < 60 \text{ cm/s}$  and  $20 \text{ cm/s} < \text{PGV} < 40 \text{ cm/s}$ , respectively. These records do not contain pulse signals. Groups C and D consist of 20 and 18 records, respectively, and exhibit pulse signals in their waveforms. The PGV values of the Group C records are in between 40 cm/s and 60 cm/s, whereas the Group D records attain PGV values greater than 60 cm/s. Group A contains larger magnitude ground motions among the records without pulse, whereas Group D ground motions are recorded at relatively closer distances among the pulse dominant records.

Fig. 1 presents the design spectra that describe the median variation of 5% damped pseudo-acceleration spectra ( $S_a$ ) of the

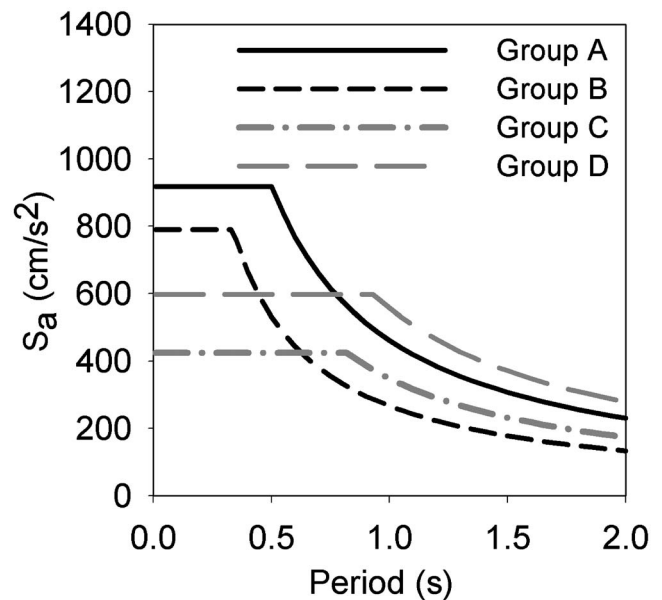
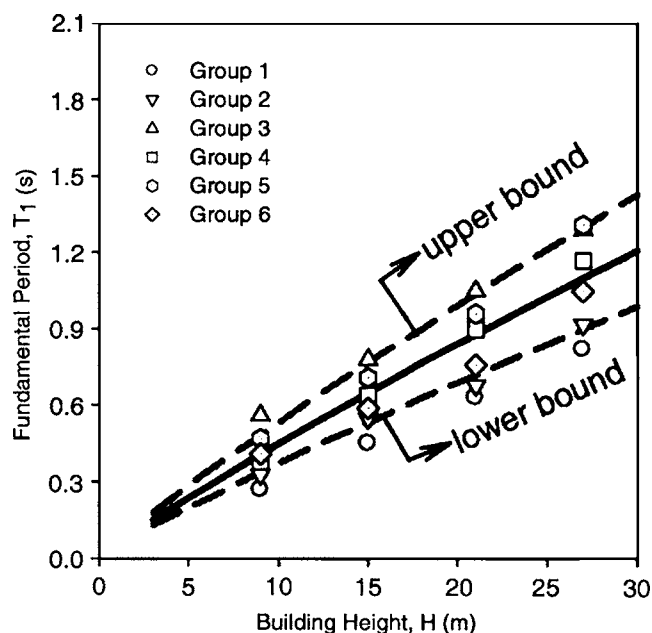


Fig. 1. Median design spectra used in the model frames

records for each bin. The spectral shapes are consistent with the magnitude and distance features of the bins. The median demands of Groups D and A are higher than those of Groups C and B, respectively, that contain longer distance (Group C) and lower magnitude (Group B) records. The corner period that separates the constant-acceleration plateau from the descending branch is shifted towards longer periods for bins that exhibit larger PGV (such as the median design spectrum of Group A against B) and/or pulse-type signals (such as the median design spectra of Groups C and D against Group A). The descending branches of Groups C and D decay relatively slower than the other two groups due to the dominant long-period pulses in their waveforms. These observations mark the salient characteristics of the near-fault events suggesting that the database can reflect almost all of the common features of the near-fault records.

## Building Models and Pushover Analyses

The median design spectrum of each ground-motion bin was used to model three bay, RC regular moment-resisting frames. The span width and story height of the buildings were chosen as 5 m and 3 m, respectively. The height-wise lateral stiffness distribution of the frames was tuned to satisfy the drift limits imposed by FEMA-450 (BSSC 2003). The dimensions and detailing of the models aim to ensure nondegrading strength behavior as the NSPs presented in FEMA-440 are evaluated for this particular case. The Kent and Park model (Kent and Park 1971) was used for the concrete stress-strain relationship that determines the ultimate deformation capacity considering the degree of confinement. The unconfined concrete compressive strength and initial Young's modulus were taken as 20 and 28,500 MPa, respectively. The concrete strain at the maximum compressive strength is 0.002. The ultimate deformation capacity of the concrete members is high due to the confinement detailing. The yield and ultimate strength capacity of the reinforcing bars are 420 MPa and 588 MPa, respectively. The initial modulus of elasticity of the reinforcing bars is 200,000 MPa. At the commencement of the strain hardening (strain values greater than 0.03) the elasticity



**Fig. 2.** Fundamental period ( $T_1$ ) versus total height ( $H$ ) scatter of the model frames superimposed by the empirical boundaries presented by Chopra and Goel (2000a)

modulus of the steel bars reduces to 1/60th of its initial value. The frames were analyzed using the software IDARC-2D (Valles et al. 1996) that is capable of fiber modeling and spread plasticity to capture the variation of section plasticity. The initial viscous damping was taken as 5% for the model buildings. (Unless stated otherwise, the initial viscous damping is 5% in all dynamic analyses that is compatible with the NSPs investigated.)

Moderate-stiffness degradation was implemented during the nonlinear RHA of the frames that is generally expected for well-designed concrete buildings during cyclic excursions. The influence of this hysteretic model on the global deformation demands was investigated by repeating the nonlinear RHA for the bilinear cyclic behavior that does not account for the stiffness degradation. The comparisons showed that the chosen hysteretic model, on average, yields peak roof displacements that are 7% larger than those computed from the bilinear hysteretic model. This difference is, on average, 8% for the peak interstory drift values. Confined to the ground motions and building models of this study, these observations may advocate that the results presented can arguably be valid for the bilinear cyclic behavior.

A total of six sets of frames were designed with three, five, seven, and nine stories covering a fundamental period range of 0.27 s–1.31 s. Fig. 2 presents the fundamental period ( $T_1$ ) versus the total height ( $H$ ) variations of the models that are fairly consistent with the empirical relationships presented by Chopra and Goel (2000a). Thus, the models used can be interpreted as the representatives of general moment-resisting RC frame behavior for three- to nine-story levels.

Table 1 lists some of the important features of model frames. The idealized period ( $T_{1,id}$ ) and the postyielding stiffness ratio ( $\alpha$ )

**Table 1.** Important Properties of Model Buildings

Building	Story number	$T_1$ (s)	Triangle		Uniform		Ground motion
			$T_{1,id}$ (s)	$\alpha$ (%)	$T_{1,id}$ (s)	$\alpha$ (%)	
Group 1	3-st.	0.27	0.27	2.3	0.25	2.2	Bin A
	5-st.	0.45	0.44	3.1	0.40	3.7	
	7-st.	0.63	0.64	4.3	0.57	4.9	
	9-st.	0.82	0.82	4.6	0.74	5.4	
Group 2	3-st.	0.33	0.31	2.3	0.31	2.6	Bin B
	5-st.	0.55	0.55	4.1	0.51	4.7	
	7-st.	0.68	0.67	3.5	0.59	3.6	
Group 3	3-st.	0.56	0.55	3.2	0.51	3.2	Bin C
	5-st.	0.78	0.78	3.8	0.70	5.5	
	7-st.	1.05	1.00	4.5	0.88	5.3	
	9-st.	1.29	1.23	5.5	1.14	5.7	
Group 4	3-st.	0.38	0.37	3.9	0.38	4.0	Bin A
	5-st.	0.64	0.65	6.3	0.59	7.6	
	7-st.	0.90	0.90	7.1	0.78	6.1	
Group 5	3-st.	0.47	0.47	4.4	0.44	4.4	Bin B
	5-st.	0.71	0.69	4.4	0.64	4.5	
	7-st.	0.96	0.93	8.2	0.83	10.5	
	9-st.	1.31	1.25	12.4	1.13	12.1	
Group 6	3-st.	0.41	0.41	2.7	0.38	2.7	Bin D
	5-st.	0.59	0.59	4.2	0.54	5.0	
	7-st.	0.76	0.76	3.5	0.69	3.9	
	9-st.	1.05	1.03	4.4	0.98	5.5	

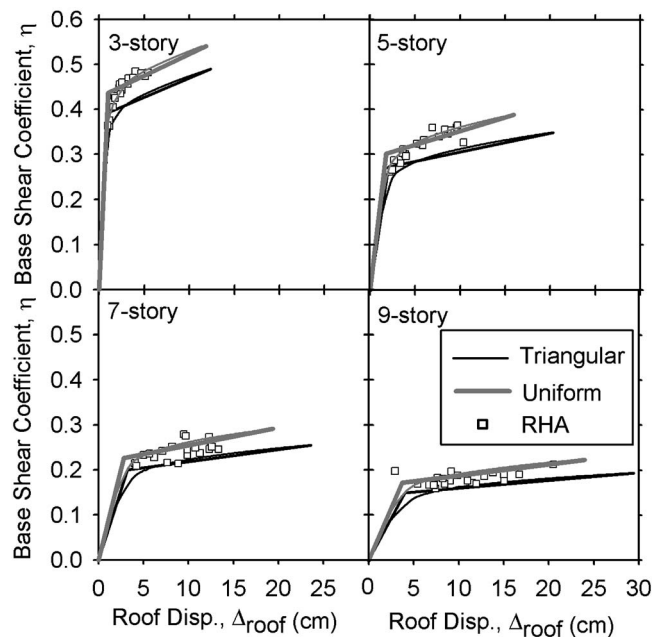


**Fig. 3.** Global capacity envelopes and corresponding bilinear idealizations of Group 1 model buildings. The plots superimpose  $\eta$ – $\Delta_{\text{roof}}$  pairs computed from nonlinear RHA.

were computed from the pushover curves. The height invariant inverse triangular and uniform loading patterns were used in the pushover (PO) analyses. The inverse triangular pattern is one of the lateral load distributions suggested by the building codes for structures deforming primarily in the first mode, and is similar to the equivalent lateral force distribution described in FEMA-356 for the building models. The uniform loading pattern implements lateral forces proportional to story masses emphasizing the demands in the lower stories. This loading pattern is suggested to be complementary to inverse triangular loading by FEMA-356 and accounts for the uncertainties in the variation of deformation demands during strong ground shaking.

When comparing PO curves with and without P-delta effects no negative postyield stiffness that ensures structural instability at high deformations was observed. This suggests minimal or no P-delta effect for the frames investigated. Thus, P-delta effects were disregarded in this study. This further simplification also avoids biased comparisons between the improved NSPs, since they consider the influence of P-delta in different ways; the improved DCM imposes a limit on lateral strength as a function of the negative postyielding stiffness ratio to prevent dynamic instability during nonlinear behavior, whereas CSM provides information on the P-delta influence via in-cycle strength degradation excursions.

The bilinear idealization of the PO curves was performed following the methodology presented in ATC-40 that is still one of the methods suggested for the improved NSPs. These curves were used in the computation of  $T_{1,\text{id}}$  and  $\alpha$ , as well as representing the idealized bilinear SDOF systems of the models. A sample illustration of the PO curves and the corresponding bilinear idealizations is presented in Fig. 3. The idealized periods computed from the inverse triangular and uniform loading patterns are fairly close to the fundamental periods of most low-rise building models. This agreement loosens for seven- and nine-story buildings, since their PO curves computed from the uniform loading pattern reveal shorter  $T_{1,\text{id}}$  with respect to those computed from the inverse tri-

angular pattern. The yield strengths computed from the uniform lateral loading attain larger values than those obtained from the inverse triangular loading. The postyield stiffness of the uniform lateral loading is generally larger than the inverse triangular loading, although, for some buildings the differences are negligible. The differences reported in the global capacity curves can emerge from the point of application of the resultant force of the lateral load patterns. The uniform loading pattern gives the lowest point of application of the resultant lateral force; hence, larger strength and earlier global yield are computed. The resultant lateral load of the inverse triangular pattern is applied at a higher point displaying lower strength, as well as higher global yield.

The maximum absolute base-shear coefficient ( $\eta$ ) versus the roof displacement ( $\Delta_{\text{roof}}$ ) pairs computed from the nonlinear RHA are also superimposed in Fig. 3. They show that the global response of the subject frames is enveloped fairly well by these two lateral loading patterns. For low-rise buildings, the uniform loading reveals fairly better representation of global response. As the number of stories increases, the RHA results fall between the envelopes dictated by these alternative loading patterns. Albeit, the apparent differences between the PO curves and  $\eta$  versus  $\Delta_{\text{roof}}$  scatters, their fairly good agreement indicates a first-mode dominant deformation of the model buildings. The postyielding stiffness ratio generally attains values in between 2%–5% that is also realistic for properly designed frame systems. However, for some frames,  $\alpha$  takes large values. This can be attributed to the high quality material properties, as well as the lateral loading patterns implemented and the bilinear idealization procedure used. Note that similar large  $\alpha$  values were also presented in the literature for well-designed concrete frames (e.g., ATC 1996). Mwafy (2001) indicated that height invariant loading patterns cannot capture the postyield stiffness accurately when compared to the nonlinear RHA.

### NSPs Presented in the FEMA-440 Report

The improved NSPs presented in FEMA-440 primarily modify the former DCM and CSM to enhance the inelastic peak SDOF displacement estimations. The improved DCM modifies  $C_1$  and  $C_2$  coefficients to improve the expected elastoplastic oscillator deformation estimations from their elastic counterparts ( $C_1$ ) and modify these estimations for cyclic degradation ( $C_2$ ). This procedure suggests eliminating coefficient  $C_3$  (used in the former version) that accounts for the amplification in deformations due to the P-delta effects. Instead, it establishes a limit on the lateral strength to avoid dynamic instability. The improved CSM proposes new effective damping and period relationships for a vast variety of cyclic behavior (bilinear, stiffness degrading, and in-cycle strength degrading) and postyield stiffness to predict the nonlinear SDOF deformation demands through an equivalent linear system. Essentially, both NSPs relate the predicted SDOF deformation demands to the MDOF behavior through some factors that rely on the first-mode shape vector and the participation factor. This section initially discusses the modifications presented in the FEMA-440 for the peak SDOF displacement prediction. Later, the relationships used for relating SDOF demands to MDOF response are discussed.

### Improved DCM to Estimate Equivalent SDOF Deformation Demands

The recommended  $C_1$  and  $C_2$  expressions for the improved DCM are

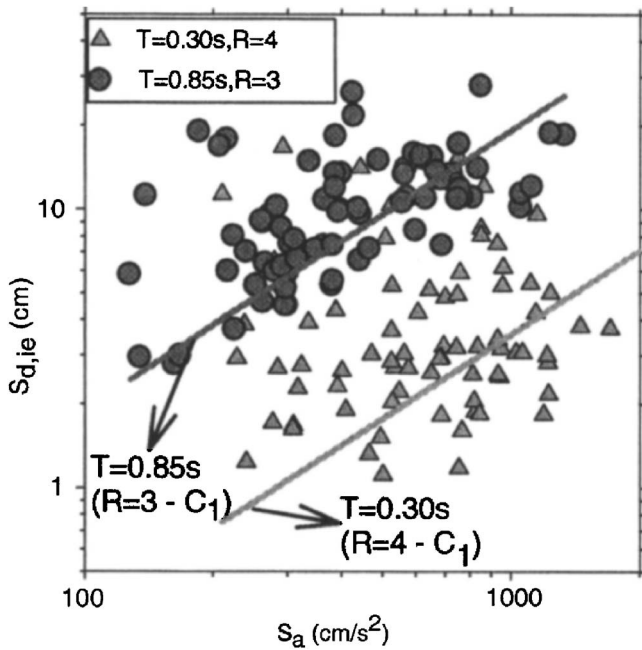


**Fig. 4.** Comparisons between the actual variation of elastoplastic  $S_{d,ie}$  (scatter plots) and corresponding estimations (solid lines) via improved  $C_1$  as a function of  $S_a$

$$C_1 = 1 + (R - 1)/(aT_e^2); \quad C_2 = 1 + 1/800((R - 1)/T_e)^2; \quad R = \frac{F_e}{F_y} \quad (1)$$

In Eq. (1)  $R$  represents the normalized lateral strength ratio and defines the yield strength ( $F_y$ ) capacity of the SDOF system relative to its elastic strength ( $F_e$ ). The elastic and yield strength capacities of the oscillators can be expressed by the corresponding elastic and yield pseudo-accelerations, respectively, when the calculations are based on mass normalized SDOF systems. The effective period term,  $T_e$ =vibration period of the SDOF system computed from the initial branch of the idealized PO curve ( $T_{1,id}$  this study). The regression constant  $a$  is devised for the influence of different site classes. Since  $C_1$  describes the expected inelastic deformation demands on the oscillators as a function of  $R$  and  $T_{1,id}$  the estimated peak SDOF response is, inherently, a linear function of the elastic pseudo-acceleration. This factor disregards the influence of the postyield stiffness that is deemed to be important for the peak displacements of short-period and low-strength oscillators (Chopra and Chintanapakdee 2004; Ruiz-García and Miranda 2003). The coefficient  $C_2$  accounts for the changes in the peak SDOF displacements produced by departures from the elastoplastic model due to severe stiffness, and/or strength degrading hysteretic behavior. It is equal to 1 for periods greater than 0.7 s in the improved DCM. This coefficient is taken as 1, since the differences in the peak roof and interstory drifts computed from the bilinear and moderate stiffness-degradation hysteretic models are found as negligible in this study.

Figs. 4 and 5 illustrate the essential implications of the above discussions using the improved  $C_1$  values. Fig. 4 shows the  $S_a$  dependent variation of the elastoplastic peak SDOF displacements ( $S_{d,ie}$ ) computed from RHA and compares them with the corresponding estimations through  $C_1$ . Note that the estimated  $S_{d,ie}$  constitutes a linear relationship with  $S_a$  based on the theory explained in the previous paragraph. The comparisons are done for

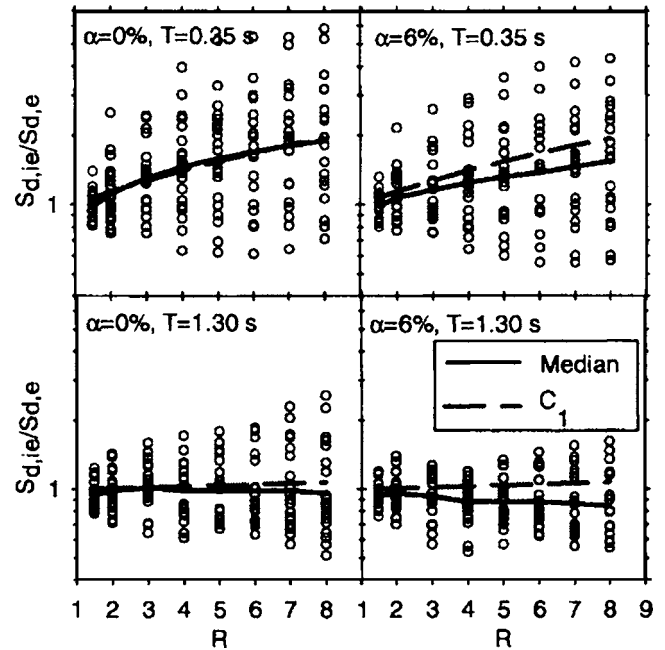


**Fig. 5.** Sensitivity of  $S_{d,ie}/S_{d,e}$  to postyielding stiffness ( $\alpha$ )

a short period ( $T=0.3$  s) and for an intermediate period ( $T=0.85$  s) oscillator response with moderate yield-strength levels represented by  $R=4$  and  $R=3$ , respectively. The actual variation of  $S_{d,ie}$  shows a significant dispersion about these linear trends particularly for the short-period oscillator. This observation indicates that seismological features affecting the nonlinear deformation demands cannot be captured accurately by modifying the elastic demands via  $C_1$ . Recent studies have shown that some ground-motion parameters play a role in the improvement of the median nonlinear deformation predictions, as well as reducing dispersion about the median estimations (e.g., Akkar and Özen 2005).

Fig. 5 presents the scatter plots for the  $S_{d,ie}/S_{d,e}$  ratios computed from the nonlinear RHA as a function of  $R$  using Group A records. The ratios are plotted for two distinct vibration periods;  $T=0.35$  s and  $T=1.3$  s, and two postyielding stiffness ratios;  $\alpha=0$  and  $\alpha=6\%$  to describe the influence of  $\alpha$  on the inelastic peak SDOF displacements. The first and second rows in Fig. 5 display the results for  $T=0.35$  s and  $T=1.3$  s, respectively. The left and right panels present  $S_{d,ie}/S_{d,e}$  ratios pertaining to  $\alpha=0$  and  $\alpha=6\%$ , respectively. The median variations of  $S_{d,ie}/S_{d,e}$  and the functional behavior of  $C_1$  are also shown in these plots. The plots indicate that improved  $C_1$  describes the median variation of  $S_{d,ie}/S_{d,e}$  fairly well for the elastoplastic behavior. However, there is a significant deviation between the median  $S_{d,ie}/S_{d,e}$  and  $C_1$  for nonzero postyield stiffness showing that the improved  $C_1$  tends to overestimate  $S_{d,ie}$  when compared to the results of RHA. The discrepancy rapidly builds up for  $R \leq 6$  and follows a more stable trend for larger  $R$ . Note that concrete structures with low yield strength may not maintain large reserved stiffness and strength capacities (mimicked by  $\alpha=6\%$ ), particularly when they are exposed to large deformation demands. This study overlooks the loss of the reserved capacity due to the strength deterioration and dictates the nonlinear response of the building models via moderate-stiffness degradation. The large normalized lateral strength values (i.e.,  $R \geq 7$ ) presented in Fig. 5 serve for completing the general view about the emphasis of  $\alpha$  on the peak inelastic SDOF displacement estimations that is disregarded by  $C_1$ .

### Improved CSM to Estimate Equivalent SDOF Deformation Demands

The improved CSM determines the equivalent linear parameters (effective period,  $T_{\text{eff}}$ , and effective damping,  $\beta_{\text{eff}}$  through a statistical analysis that minimizes the extreme differences between the maximum response of an actual inelastic SDOF system and its equivalent linear counterpart (Guyader and Iwan 2006). In the improved CSM, both  $T_{\text{eff}}$  and  $\beta_{\text{eff}}$  expressions are discontinuous at two distinct ductility values ( $\mu=4$  and  $\mu=6.5$ ), and they are suggested to be used for  $\mu$  less than 10–12. The format of  $T_{\text{eff}}$  and  $\beta_{\text{eff}}$  expressions is given in Eqs. (2)

$$\beta_{\text{eff}} = A(\mu - 1)^2 + B(\mu - 1)^3 + \beta_0;$$

$$T_{\text{eff}} = [G(\mu - 1)^2 + H(\mu - 1)^3 + 1]T_0 \quad \mu < 4 \quad (2a)$$

$$\beta_{\text{eff}} = C + D(\mu - 1) + \beta_0; \quad T_{\text{eff}} = [I + J(\mu - 1) + 1]T_0$$

$$4.0 \leq \mu \leq 6.5 \quad (2b)$$

$$\beta_{\text{eff}} = E \left[ \frac{F(\mu - 1) - 1}{F(\mu - 1)^2} \right] \left( \frac{T_{\text{eff}}}{T_0} \right) + \beta_0;$$

$$T_{\text{eff}} = \left\{ K \left[ \sqrt{\frac{(\mu - 1)}{1 + L(\mu - 2)}} - 1 \right] + 1 \right\} T_0 \quad \mu > 6.5 \quad (2c)$$

The parameters  $T_0$  and  $\beta_0$ =initial period and viscous damping of the bilinear SDOF system idealized from the PO curves. The constants  $A$  through  $K$  vary for different  $\alpha$  values and hysteretic models. The improved CSM also presents alternative values for these constants that can be used for any case regardless of  $\alpha$  and hysteretic model.

Iterative or graphical procedures are required in CSM to estimate the peak nonlinear SDOF displacements, since  $\beta_{\text{eff}}$  and  $T_{\text{eff}}$  are functions of  $\mu$  that is not known a priori from the idealized PO curves. The effective period expressions in the improved CSM do not follow the secant-stiffness approach that was the case in the former version presented in ATC-40. This fact complicates the graphical solution. Therefore, in this study, the direct iteration (Procedure A) technique was used to estimate the peak nonlinear SDOF displacements by the improved CSM. The procedure starts with an initial assumption for the displacement ductility ( $\mu_{\text{initial}}$ ), computes the equivalent linear parameters using Eqs. (2), and estimates the peak SDOF displacement from the equivalent linear system. This estimation is used to compute the new displacement ductility ( $\mu_{\text{computed}}$ ). The initial and computed ductilities are then compared and the absolute relative difference between  $\mu_{\text{initial}}$  and  $\mu_{\text{computed}}$  is used as the criterion for finalizing the computations. If it is less than a given tolerance level, the computations are terminated. Otherwise, the initial ductility is set to the value of  $\mu_{\text{computed}}$  and the iterations continue until  $\mu_{\text{initial}}$  and  $\mu_{\text{computed}}$  converge satisfying the predetermined tolerance level. The iterative schemes are numerical methods, and they aim to approach the root(s) of a function. The convergence between the consecutive iterations warrants the satisfactory approximation to the root that is dictated by the tolerance level. The particular iterative scheme described here may run into oscillating divergence problems (Chopra and Goel 2000b) that can be treated by some numerical analysis techniques (Miranda and Akkar 2002).

Two typical oscillating divergence cases experienced during the implementation of the improved CSM method are presented in Fig. 6. In the left panel, the initially assumed ductility  $\mu_{\text{initial}}=2$  diverges towards the ductility value of 3, and later, an infinite

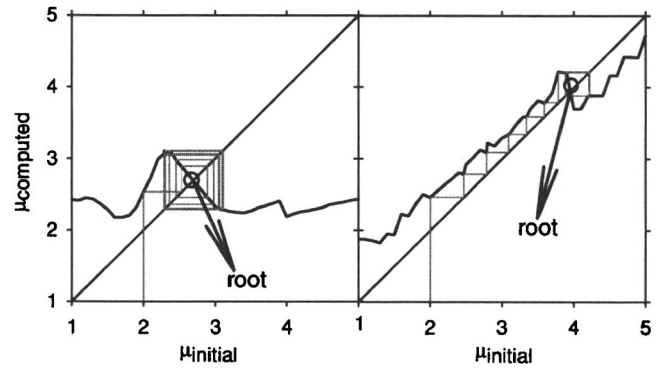


Fig. 6. Oscillating-divergence type numerical problems experienced in the improved CSM

oscillation occurs between two ductility points. This ill-case can be cured by applying the interval halving that would result in a quick convergence to the root (peak SDOF displacement estimation). The second example on the right panel is another illustration for infinite oscillation due to the discontinuity in Eqs. (2a)–(2c) at  $\mu=4$  that appears as an abrupt change in the functional form in the vicinity of  $\mu=4$ . For this particular case, the iterative scheme initially displays a converging behavior towards the root, but the discontinuity in the vicinity of  $\mu=4$  results in an infinite oscillation between two particular ductility values. This numerical problem can also be solved by the application of interval halving.

Fig. 7 shows a comparison between the ductility demands computed from the nonlinear RHA (designated as  $\mu_{\text{exact}}$ ), and the iterative procedure used in this study ( $\mu_{\text{approx}}$ ). The idealized bilinear PO curves obtained from the triangular and uniform loading patterns that represent the model frames were used in the nonlinear RHA to compute  $\mu_{\text{exact}}$ . The  $\mu_{\text{approx}}$  corresponds to the ductility when the improved CSM converges to the approximate peak SDOF displacement via Eqs. (2a)–(2c) for a tolerance level

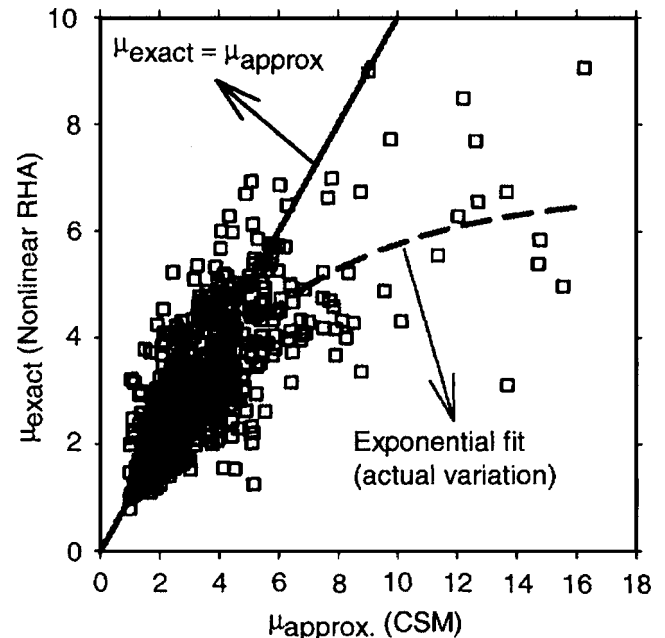
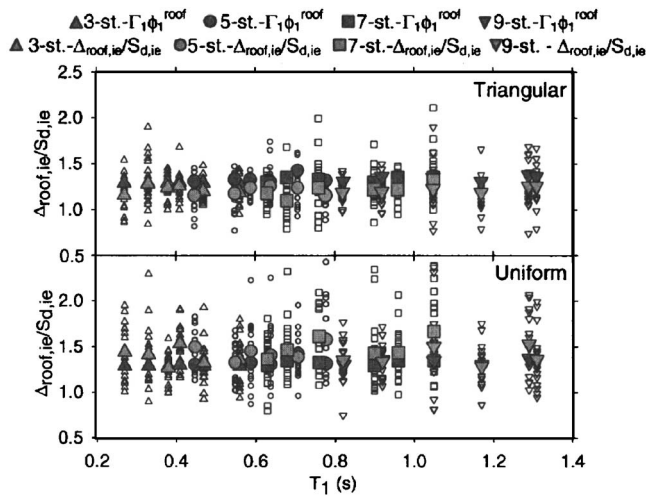


Fig. 7. Scatter diagram for  $\mu_{\text{exact}}$  versus  $\mu_{\text{approx}}$  computed from nonlinear RHA and CSM, respectively



**Fig. 8.**  $\Delta_{\text{roof,ie}}/S_{d,ie}$  scatters associated with their median values for each building model computed from nonlinear RHA. Comparisons with the corresponding elastic  $\Gamma_1\phi_1^{\text{roof}}$ .

of 5%. The scatter diagram in Fig. 7 indicates that the ductility demand estimations of the improved CSM are in good agreement with  $\mu_{\text{exact}}$  for  $\mu \leq 4$ . As  $\mu_{\text{exact}}$  attains higher values, this agreement loosens. The estimations of the improved CSM attain larger values than the nonlinear dynamic analyses. This is emphasized by the exponential fit between  $\mu_{\text{exact}}$  and  $\mu_{\text{approx}}$ .

### Transforming Equivalent SDOF Deformation Estimates to MDOF Systems

The prime assumption in the NSPs is that the behavior of MDOF systems can be anticipated from the response of the SDOF systems. In most cases, the response of the bilinear SDOF system is related to the MDOF system via the first-mode elastic dynamic properties as described in ATC-40 and FEMA-356 (designated as  $C_0$  in DCM). FEMA-440 does not attempt to propose a new relationship for modifying the SDOF demand estimations for MDOF behavior. The statistical studies conducted in FEMA-440 using a total of 11 far-fault and 4 near-fault records for 5 example buildings indicated that the peak roof displacements would be overestimated by 10–20% when the peak SDOF displacements computed from the nonlinear RHA are modified by the product  $\Gamma_1\phi_1^{\text{roof}}$  (elastic first-mode participation factor,  $\Gamma_1$ , multiplied by the amplitude of first-mode vector at the roof,  $\phi_1^{\text{roof}}$ ). Alternative to  $\Gamma_1\phi_1^{\text{roof}}$ , FEMA-356 also tabulates some coefficients to modify the peak SDOF displacement for the roof displacement. These coefficients depend on the story number and the lateral loading pattern used during the PO analysis.

This study conducted a statistical analysis using the ratios of the peak roof displacements of the building models ( $\Delta_{\text{roof,ie}}$ ) to the peak SDOF displacements ( $S_{d,ie}$ ) computed from the nonlinear RHA. The idealized bilinear SDOF systems computed from the triangular and uniform lateral loading patterns were used to compute  $S_{d,ie}$ . The ratio,  $\Delta_{\text{roof,ie}}/S_{d,ie}$  yields an empirical relationship for SDOF to MDOF global deformation demand variation.

The top and bottom scatter diagrams given in Fig. 8 display the variations of  $\Delta_{\text{roof,ie}}/S_{d,ie}$  for the triangular and uniform lateral loadings, respectively. Each vertical strip corresponds to the results from a particular building model excited by the records of the corresponding ground-motion bin. The median  $\Delta_{\text{roof,ie}}/S_{d,ie}$  variation of each vertical strip (filled with light gray color) is

incorporated into these plots. The factor  $\Gamma_1\phi_1^{\text{roof}}$  computed from the elastic dynamic properties of each model frame (filled with a darker color scheme) is also presented in these diagrams. Fig. 8 reveals that elastic  $\Gamma_1\phi_1^{\text{roof}}$  would be misleading for relating the SDOF response to MDOF response in the nonlinear range. Different lateral loading patterns used in computing the idealized SDOF systems dictate different  $\Delta_{\text{roof,ie}}/S_{d,ie}$  ratios. Comparisons between the median  $\Delta_{\text{roof,ie}}/S_{d,ie}$  and  $\Gamma_1\phi_1^{\text{roof}}$  suggest that the use of the latter factor would result in conservative roof displacement estimations for the analyses that are based on the triangular loading pattern, because the median  $\Delta_{\text{roof,ie}}/S_{d,ie}$  yields relatively lower values than  $\Gamma_1\phi_1^{\text{roof}}$ . When the analyses that are based on the uniform lateral loading are of concern, the use of the  $\Gamma_1\phi_1^{\text{roof}}$  would, on average, result in lower roof displacement predictions with respect to nonlinear MDOF dynamic analyses, since median  $\Delta_{\text{roof,ie}}/S_{d,ie}$  ratios mostly constitute the upper bound when compared to the  $\Gamma_1\phi_1^{\text{roof}}$  values. The median  $\Delta_{\text{roof,ie}}/S_{d,ie}$  ratios mostly fluctuate about a value of 1.2 for the triangular loading pattern. The same median ratios outline a more complex pattern for the uniform lateral loading attaining values generally greater than 1.3 and having a tendency towards higher values with an increasing fundamental period. Scatters for uniform loading also display a more dispersive character towards longer periods. As discussed previously, the increased discrepancy between the fundamental periods of taller building models and  $T_{1,id}$  recomputed from uniform lateral loading can be the main reason behind this observation.

Based on the statistics discussed above, the use of the first-mode shape and modal participation factor at the level of the estimated peak SDOF displacement would be more convenient for NSPs, while relating the SDOF demands to the MDOF response. This way, the MDOF deformation estimations can take into account the time-dependent deflection profile of structures responding beyond their elastic limits. The above information can be extracted from the PO database. It is believed that the application of this procedure would reduce the bias in global deformation demand estimations derived from the SDOF deformation predictions when compared to the direct use of elastic  $\Gamma_1\phi_1^{\text{roof}}$ .

### Error Statistics

Inelastic peak displacements of idealized bilinear SDOF systems, peak roof, and interstory drifts computed from nonlinear RHA were used to verify the performance of improved NSPs. Deformation demands computed from the nonlinear RHA were assumed to be “exact” and compared to the predictions of the improved CSM and DCM. The  $R$ -values computed from each idealized bilinear oscillator ground-motion pair were implemented to the improved  $C_1$  to estimate the inelastic peak SDOF displacements [ $(S_{d,ie})_{\text{approx}}$ ]. The constant  $a$  in the improved  $C_1$  was taken as 60, because almost all ground motions are recordings from stiff soil sites. For the improved CSM, the iterative procedure described in the previous section was employed to compute  $(S_{d,ie})_{\text{approx}}$  for each particular case. The expressions presented in Eqs. (2a)–(2c) were implemented using the hysteretic model and postyield stiffness independent constants. A tolerance level of 5% was used for terminating the iterations in the improved CSM. In oscillating divergence cases, the interval halving method was used. The fundamental mode shape and corresponding modal participation factor inferred from the PO database at the estimated peak SDOF displacement were used in predicting the peak roof and interstory drifts.

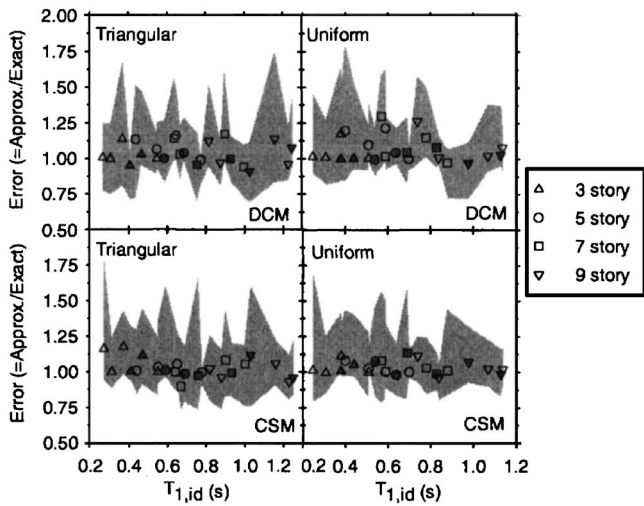


**Fig. 9.** Median error scatters and associated dispersion for spectral displacement estimations using the improved DCM (upper row) and CSM (lower row)

The error statistics were derived by computing the ratios of predicted response quantities to the corresponding exact values determined from the nonlinear RHA. The NSPs underestimate the median response quantity if the median ratio computed from these error terms is less than one, and provide an overestimation if this ratio exceeds one. The median error and the pertaining dispersion (16th and 84th percentiles) were computed for each building model subjected to the records of the corresponding ground-motion bin. The error statistics (Figs. 9–11) are presented by making use of scatter plots that describe the variation of median errors. Different symbols describe the statistics corresponding to different story numbers (statistics pertaining to pulse-dominant records are distinguished from the rest by symbols filled with a darker color scheme). The gray shaded region in each plot represents the area bounded by 16th and 84th percentiles of error statistics. They describe the dispersion on the deformation demand estimations. The first row in each figure presents the error statis-

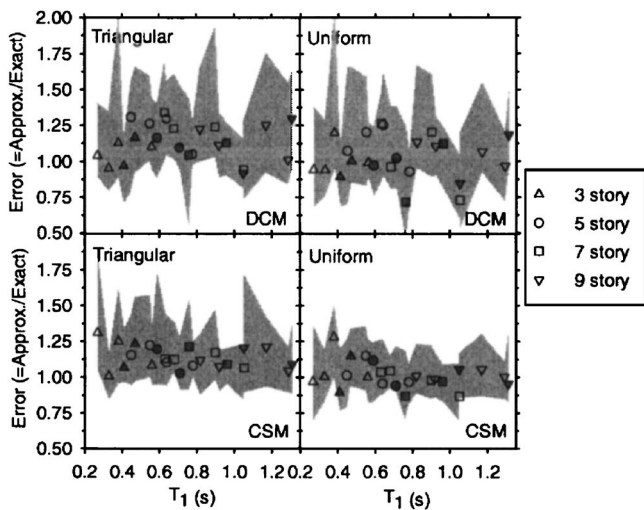


**Fig. 10.** Median error scatters and associated dispersion for peak roof displacement estimations using the improved DCM (upper row) and CSM (lower row)

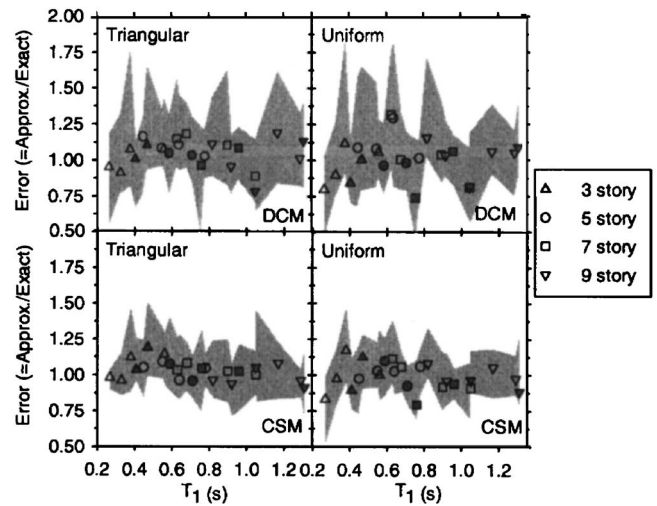


**Fig. 11.** Median error scatters and associated dispersion for peak interstory drift estimations using the improved DCM (upper row) and CSM (lower row)

tics for the improved DCM. The second rows display the error statistics of the improved CSM. The error statistics of the triangular and uniform loading patterns are presented in the first and second columns of each figure, respectively.

Median errors in Fig. 9 indicate that on average both NSPs would have a  $\pm 10\%$  error range in estimating the peak SDOF displacements of the bilinear systems idealized from the inverse triangular loading. For  $T_{1, id} > 0.6$  s, the improved DCM yields slightly larger  $(S_{d, ie})_{approx}$ , since the pertaining median errors attain values greater than 1.1. This trend is reversed for short periods (i.e.,  $T_{1, id} < 0.4$  s) displaying median errors greater than 1.1 for the improved CSM. Both NSPs display fairly better inelastic peak SDOF displacement estimations for the uniform lateral loading that is particularly valid for the improved CSM. For this lateral loading pattern, the median peak SDOF displacement estimations of DCM are larger than 20% from those of the nonlinear RHA for some individual cases. Improvements in peak SDOF displacement estimations for uniform lateral loading may originate from the relatively higher yield strength values of the idealized PO curves with respect to those computed from the inverse triangular loading. Higher yielding strength that results in lower  $R$  seems to improve  $(S_{d, ie})_{approx}$ . Dispersion about the median errors suggests that both NSPs may introduce significant uncertainty in the peak SDOF displacement estimations. The dispersion about the median error is slightly larger for the improved DCM. This can be attributed to the lack of consideration of  $\alpha$  on the peak SDOF estimations and their linear dependency on  $S_a$  that are discussed within the context of Figs. 4 and 5.

Median errors presented for peak roof displacements in Fig. 10 indicate that, in the case of the inverse triangular loading, both NSPs would tend towards more conservative estimations. The tendency in overestimation is more noticeable for the improved DCM. The loading sequence introduced by the inverse triangular pattern can be the major reason behind the increased overestimations. This loading pattern promotes larger roof displacements, since it dictates uniformly increasing lateral deformations regardless of the structural response in the elastic or beyond the elastic range. However, as the structure responds beyond the elastic range, the concentration of plastic hinging at lower stories would not permit very high roof displacements. The error statistics com-

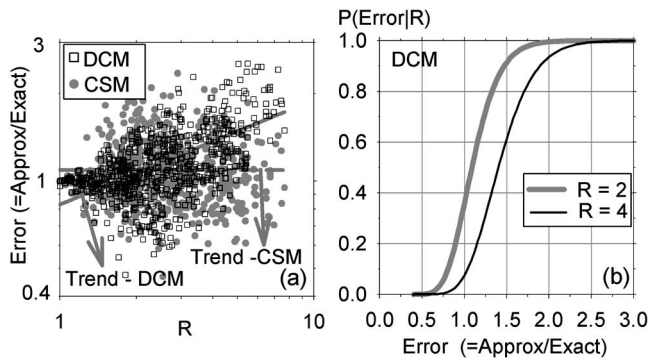


**Fig. 12.** (a) Variation of error trends in spectral displacement estimations as a function of normalized lateral strength ratio  $R$  for improved DCM and CSM; (b) log-normal probability distributions of error conditional to  $R$  for improved DCM

puted for the uniform loading resemble fairly better performance for both NSPs with median estimations mostly bounded between  $\pm 10\%$  range with respect to those of the nonlinear RHA. For this loading pattern, the median errors that reveal underestimation of roof displacements generally belong to the relatively long-period building models subjected to records with pulse. The dispersion about the median error for uniform loading is also reduced when compared to the dispersion associated with inverse triangular loading. This observation is more noticeable for the improved CSM. Note that regardless of the lateral loading pattern the dispersions associated with the improved DCM are larger than those of the improved CSM.

The median error statistics presented for peak interstory drift estimations in Fig. 11 reveal similar conclusions to those described for peak roof displacements. When inverse triangular loading is considered, the median errors show that peak interstory drifts would be overestimated by a maximum amount of 25% by both NSPs. The overestimations are larger in the improved DCM. The median interstory drift estimations are slightly improved for uniform lateral loading, since most median errors clustered in between 0.9–1.1. The uniform loading pattern emphasizes deformation demands in the lower stories that can be a major factor for the improvements in the median peak interstory drift estimations. This loading pattern also results in a reduction about the uncertainty in peak interstory drifts estimated by the improved CSM. The enhancement in median interstory drift estimations by the improved DCM via uniform loading is not reflected to the corresponding dispersion statistics. The dispersions about the median errors in this method are significant for both the inverse triangular and uniform loading patterns. Note that, for both NSPs, the error statistics of records with pulse have a tendency towards the unsafe side for increasing  $T_1$ .

The dispersion about the median error statistics is further investigated by plotting the error scatters of the peak inelastic SDOF displacement estimations as a function of  $R$  for both NSPs. Fig. 12(a) presents the corresponding scatters that are plotted from the error statistics of the records without pulse. The error scatters and the associated regression fits displayed in Fig. 12(a) indicate that the peak SDOF displacement estimations of improved DCM are biased towards the conservative side with increasing  $R$  values. The same trend is not observed for the improved CSM, since the associated errors follow a random pattern about the regression line fitted for the CSM statistics.

Based on the above discussions and assuming log normal dis-

tribution, the error probability distributions conditional to  $R$  were calculated for the improved DCM to investigate the degree of  $R$  dependency on the corresponding peak SDOF displacement estimations. The theoretical background of this second-order probabilistic approach is given in Giovenale et al. (2004). Fig. 12(b) presents an illustrative example that shows the corresponding error cumulative distribution functions (CDFs). The CDFs presented indicate that the increase in  $R$  increases the possibility of having conservative peak SDOF estimations from the improved DCM. The probability of having  $P(\text{Error} > 1.3)$  (considered as the commencement of conservative estimations) is 23% for  $R = 2$ , whereas this probability is 53% for  $R = 4$ .

## Summary and Conclusions

This study evaluates the recently improved NSPs that are presented in FEMA-440. The evaluations are based on three- to nine-story, RC moment-resisting frames that are subjected to near-fault records with and without pulse signals. The buildings are regular systems and deform primarily under the fundamental mode. They conform to seismic design codes that lead to nondeteriorating lateral strength capacity due to cyclic excursions. Bilinear idealization of global building capacities was approximated using inverse triangular and uniform lateral loadings to investigate their influence on the performance of improved NSPs. The fundamental period versus building height relationship, as well as the ground-motion database featuring salient seismological characteristics of near-fault records, may suggest the generality of discussions for well-designed, low-to-medium height concrete frames subjected to near-fault records.

The improved DCM uses empirical factors to estimate the nonlinear deformation demands, and it does not account for the influence of  $\alpha$  (postyielding stiffness ratio) that reduces the deformation demands. The underlying theory of this method describes a linear relationship between the peak SDOF displacement estimation and  $S_a$ . This fact seems to fail capturing the variations in actual inelastic deformation demands that are influenced by the seismological features of ground motions. The improved CSM that considers the influence of  $\alpha$  may run into numerical problems due to the iterative process implemented. These numerical problems can be solved by applying the root finding techniques such as interval halving. The deformation demand predictions by this method are sensitive to ductility; higher  $\mu$  results in conservative predictions.

Statistics on transforming the SDOF deformations to MDOF response show that the use of first-mode elastic dynamic properties would not adequately simulate the deformation profile when structures respond beyond their elastic limits. This study used the fundamental mode properties of the model buildings at the level of peak SDOF displacement estimations to modify the SDOF behavior for the MDOF response.

The error statistics presented indicate that the improved NSPs would yield reasonably good deformation demand estimations on the median for the near-fault records without pulse. In the case of near-fault records with pulse, the NSPs investigated tend to underestimate the peak roof and interstory drift for the increasing fundamental period. The lateral loading patterns that are used for approximating the bilinear idealization of MDOF systems play a role on the accuracy of these estimations. Confined to the cases presented here, inverse triangular lateral loading generally results in more conservative estimations with respect to those of the uniform lateral loading pattern. Having a regular structural configu-

ration with fundamental periods less than 1.3 s, the model buildings deform dominantly in the first-mode promoting the concentration of plastic hinging in the lower stories. This behavior seems to be captured better by the uniform lateral loading. The lack of consideration of  $\alpha$  as well as the linear dependency of the inelastic peak SDOF displacement estimations on  $S_a$  are believed to be the important factors for the improved DCM that result in relatively conservative estimations associated with higher dispersions. The improved CSM considers the effect of  $\alpha$  on SDOF deformations. Peak nonlinear oscillator displacement estimations by CSM are carried for each record through a set of equivalent linear systems that may indicate a fairly better consideration of record-to-record variability. Error statistics conditional to  $R$  show that DCM is biased towards conservative estimations for increasing  $R$  that may contribute to the higher dispersions about the median displacement estimations. The results presented indicate that future inelastic deformation demand predictions should be explicitly based on nonlinear structural behavior, as well as the important ground-motion parameters (i.e., magnitude, site class, source-to-site distance, etc.) to reduce the biases discussed in the text.

## Acknowledgments

This study was funded by the Scientific and Technological Research Council of Turkey under Award No. 104M567. The comments of three anonymous reviewers significantly improved the technical essence and presentation quality of this article. Records used in this study were downloaded from the COSMOS website. Professors A. Erberik and G. Özcebe gave valuable information about the influence of lateral loading patterns on global capacity envelopes.

## References

- Akkar, S., and Özen, Ö. (2005). "Effect of peak ground velocity on deformation demands for SDOF systems." *Earthquake Eng. Struct. Dyn.*, 34, 1551–1571.
- Akkar, S. D., and Miranda, E. (2005). "Statistical evaluation of approximate methods for estimating maximum deformation demands on existing structures." *J. Struct. Eng.*, 131(1), 160–172.
- American Society of Civil Engineers (ASCE). (2000). "Prestandard and commentary on the seismic rehabilitation of buildings." *Rep. No. FEMA 356*, Washington, D.C.
- Applied Technology Council (ATC). (1996). "Seismic evaluation and retrofit of concrete buildings." *Rep. No. ATC-40*, Applied Technology Council, Redwood City, Calif.
- Applied Technology Council (ATC). (2005). "Improvement of nonlinear static seismic analysis procedures." *Rep. No. FEMA-440*, Washington, D.C.
- Bray, J. D., and Rodriguez-Marek, A. (2004). "Characterization of forward directivity ground motions in the near-fault region." *Soil Dyn. Earthquake Eng.*, 24, 815–828.
- Building Seismic Safety Council (BSSC). (1997). "NEHRP guidelines for the seismic rehabilitation of buildings." *Rep. FEMA-273 (Guidelines) and Rep. FEMA-274 (Commentary)*, Washington, D.C.
- Building Seismic Safety Council (BSSC). (2003). "NEHRP recommended provisions for seismic regulations for new buildings and other structures." *Rep. No. FEMA-450*, Washington, D.C.
- Chopra, A. K., and Chintanapakdee, C. (2004). "Inelastic deformation ratios for design and evaluation of structures: Single-degree-of-freedom bilinear systems." *J. Struct. Eng.*, 130(9), 1309–1319.
- Chopra, A. K., and Goel, R. K. (2000a). "Building period formulas for estimating seismic displacements." *Earthquake Spectra*, 16(2), 533–536.
- Chopra, A. K., and Goel, R. K. (2000b). "Evaluation of NSP to estimate seismic deformation: SDF systems." *J. Struct. Eng.*, 126(4), 482–490.
- Giovenale, P., Cornell, C. A., and Esteva, L. (2004). "Comparing the adequacy of alternative ground motion intensity measures for the estimation of structural responses." *Earthquake Eng. Struct. Dyn.*, 33, 951–975.
- Guyader, A. C., and Iwan, W. D. (2006). "Determining equivalent linear parameters for use in a capacity spectrum method of analysis." *J. Struct. Eng.*, 132(1), 59–67.
- Kazaz, İ., Yakut, A., and Gülkan, P. (2006). "Seismic response assessment of a stiff structure." *Earthquake Eng. Struct. Dyn.*, 35, 737–759.
- Kent, D. C., and Park, R. (1971). "Flexural members with confined concrete." *J. Struct. Div.*, 97(7), 1969–1990.
- Miranda, E., and Akkar, S. D. (2002). "Evaluation of approximate methods to estimate target displacements in nonlinear static procedures." *Proc., 4th U.S.-Japan Workshop on Performance-Based Earthquake Engineering Methodology for Reinforced Concrete Building Structures*, *Rep. No. PEER-2002/21*, Pacific Earthquake Engineering Research Center, Univ. of California, 75–86.
- Mwafy, A. M. (2001). "Seismic performance of code designed RC buildings." Ph.D. thesis, Dept. of Civil and Environmental Engineering, Imperial College, London.
- Ruiz-García, J., and Miranda, E. (2003). "Inelastic displacement ratios for evaluation of existing structures." *Earthquake Eng. Struct. Dyn.*, 32, 1237–1258.
- Valles, R. E., Reinhorn, A. M., Kunnath, S. K., Li, C., and Madan, A. (1996). "IDARC-2D version 4.0: A program for the inelastic damage analysis of buildings." *Rep. No. NCEER 96-0010*, State University of New York at Buffalo, N.Y.